

Influence of materials and geometry on fields produced by cochlear electrode arrays

H. A. Ruddy G. E. Loeb

Bio-Medical Engineering Unit, Queen's University, Kingston, Ontario K7L 3N6, Canada

Abstract—Most cochlear prostheses use multichannel electrode arrays implanted in the scala tympani to generate multiple parallel channels of activity in the tonotopically mapped auditory nerve. Various materials and geometrical arrangements of contacts and locations within the scala tympani have been used, resulting in substantial differences in the required stimulus strengths and resulting spatial distributions of neural activity. Activated iridium (AIR) permits systematic adjustment of its metal-electrolyte interface properties by changing the degree of electrochemical activation. Planar equivalent models of bipolar cochlear electrode geometries using iridium have been built, and their impedance magnitude and phase versus frequency for various degrees of activation have been characterised. The electrical fields produced at various distances from bipolar contacts in saline are measured. In comparison to platinum and unactivated iridium, AIR provides a much lower metal-electrolyte interfacial impedance. When two AIR contacts are placed with their edges close together, the resulting field distributions are determined largely by the high (but safe) current densities at their apposed edges rather than the overall extent of the contacts. These edge effects permit a novel design for a bipolar array that produces N channels of radially distributed, non-overlapping fields and that requires only $N + 1$ contacts.

Keywords—Cochlear prosthesis, Electrical fields, Electrical stimulation, Electrodes, Iridium, neural prosthesis, platinum

Med. & Biol. Eng. & Comput., 1995, 33, 793–801

1 Introduction

THE ABILITY of a stimulating electrode to activate neurons in a spatially defined region of the nervous system is essential to the performance of most neural prosthetic devices. The spread of activation depends on the dimensions and electrical properties of the nearby neurons, the amplitude and waveform of the electrical stimulus, and the distribution of the electrical fields that are created in the tissues around the electrodes (RANCK, 1975). One well known way to modify the shape and extent of the electrical fields is through the orientation of the two electrode contacts required to complete the circuit between the electronic circuitry and the body fluids. For example, 'monopolar stimulation' uses a single, usually small, contact paired with a large 'indifferent' contact, creating a spherical gradient of potentials around the monopolar contact (assuming an isotropic conductance in the surrounding tissue); 'bipolar stimulation' uses a closely spaced pair of contacts, which

causes the potential gradients to be asymmetrical and much steeper near the electrode pair.

This paper is primarily concerned with the characteristics of electrodes used for the prosthetic stimulation of the cochlea, in which spatial selectivity over a wide range of electrical waveforms is particularly important. Naturally occurring acoustic stimuli consist of many frequency components, each of which stimulates a particular location along the cochlea in a regular tonotopic progression. Most cochlear prostheses employ intracochlear electrode arrays with multiple contacts distributed over the first 18–25 mm of the scala tympani. Often several such sites are stimulated simultaneously with complex waveforms derived from the acoustic signals (LOEB *et al.*, 1983). The design and performance of such a prosthesis is improved if each site functions as an independent channel of information from the electronic circuitry to the nervous system (MERZENICH *et al.*, 1979). Previous analyses of this problem have focused on the geometrical relationships between the excitable neural processes and the electrode contacts, which are usually assumed to act like point sources (EDDINGTON, 1980). More recently, finite element models have permitted analysis of the effects of the highly heterogeneous conductances presented by the various tissues around the electrode arrays (FINLEY, 1989; FINLEY *et al.*, 1990). This paper focuses on the interaction between the reactive impedance presented by various metal-electrolyte interfaces and the conductivity of the

Correspondence should be addressed to Dr. Gerald E. Loeb, Abramsky Hall, Queen's University.

H. A. Ruddy is currently at the Department of Neurophysiology and Research Computing, Montreal Neurological Institute, Montreal, Quebec H3A 2B4, Canada.

First received 14 June 1994 and in final form 3 April 1995

© IFMBE: 1995

fluid immediately surrounding the electrode array, which can be used to improve the spatial selectivity and lower the power consumption of cochlear electrodes.

Metal-electrolyte interfaces in general are highly non-linear (GEDDES *et al.*, 1970). They have been modelled by a series resistance and capacitance (the so-called Warburg elements, often identified as R_w and C_w) in parallel with a second resistance (MAYER *et al.*, 1992); the values of all three elements are dependent on frequency and current density of an applied waveform (GEDDES, 1972; ONARAL and SCHWAN, 1982). It is not possible to characterise a metal electrode with a single time constant because this 'constant' depends on method of measurement, e.g. sinusoidal, constant current, constant voltage etc. (DE BOER and VAN OOSTEROM, 1978). The actual values depend also on the state of polarisation of the metal with respect to the electrolyte. Therefore, we have measured the impedance characteristics for symmetrical, bipolar pairs of pure platinum (Pt), non-activated iridium (NAIR) and activated iridium (AIR) contacts for a wide range of sinusoidal frequencies at charge densities similar to those used in cochlear prostheses. This permits the metal-electrolyte interfaces to settle to whatever conditions are likely to prevail in clinical devices, without any attempt to manipulate such conditions as is typically done in electrochemical studies.

The metal-electrolyte interface has been studied extensively in order to understand and to avoid electrochemical reactions that tend to damage the surrounding tissues and the electrode contacts themselves. This has led to the concept of limiting charge density and to the selection and development of materials such as AIR, which permit much higher charge density before reaching potentials at which irreversible and damaging electrochemical reactions occur (ROBBLEE *et al.*, 1983). In turn, this has led to the recognition that current density may not be distributed uniformly over the surfaces of electrode contacts (SUESSERMAN *et al.*, 1991), particularly when they are used in closely spaced bipolar pairs. The actual distribution of current and of the resulting potential gradients around the electrodes depends on the details of the metal-electrolyte interface and the electrode geometry, particularly for low impedance interfaces such as AIR (GLARUM and MARSHALL, 1980). Therefore, we measured the potential gradients around idealised versions of iridium electrode arrays with dimensions and geometries of interest for cochlear prostheses.

2 Characterisation of electrode materials

2.1 Electrode characterisation bath

A characterisation bath was designed to characterise electrode materials independently of electrode geometry and to remove the effects that occur at the edges of the electrodes. The bath contains two electrodes, made by mounting squares of the test material (Pt and Ir foils with specular reflective surface) onto flat Perspex plates. The electrodes are clamped to the ends of a Perspex cylinder (1 cm internal diameter \times 1.6 cm long). A hole tapped into the side of the Perspex cylinder permits the cavity to be filled without air bubbles and sealed with a plastic set screw. The fluid used in this bath is unbuffered mammalian normal saline (NS; 0.9 g dl⁻¹ NaCl) in order to guarantee a constant resistivity of 65 Ω cm.

2.2 Preparation and activation of electrodes

All electrodes discussed throughout this paper were cleaned electrolytically by applying -9 VDC for approximately 10 min in isotonic phosphate-buffered saline (PBS; 0.1 M

phosphate buffer and 0.128 M saline, titrated to pH 7.4). This has the effect of stripping any oxides or activation layers that may have been left on the metal surface.

The iridium electrodes, described as AIR in these experiments, were activated using cyclic voltammetry (ROBBLEE *et al.*, 1983) in PBS. They were cycled for 50 min at a rate of 0.5 V s⁻¹ between the polarisation voltages at which abrupt increases in current signalled electrolysis of water (approximately ± 0.8 V versus calomel reference electrode; the actual values tend to vary with the geometry of the electrode). This produces about a ten-fold increase in charge-carrying capacity, as indicated by the enclosed area of the current versus voltage plot from the voltammogram.

2.3 Impedance spectroscopy

Pt and Ir form largely capacitive interfaces with the electrolyte, and so both the amplitude and the phase angle of the reactive impedance (1 Hz-5 kHz) were measured by a TF2000 frequency analyser.* The 2.2 k Ω series resistor (Fig. 1a) was chosen to be much larger than the impedance of the bath under all conditions, resulting in a current-regulated waveform. The current amplitude was monitored by measuring the voltage across this resistor, and the generator voltage was adjusted to achieve a constant charge density for all frequencies (0.040 mC cm⁻² phase⁻¹). This is well within the safe range for all of these metals and approximates the usual conditions of use for cochlear electrodes. Fig. 1b shows the vector decomposition of the measured amplitudes and phases to identify the resistive and reactive (capacitive) components of the two electrode contacts (assumed to be identical) after subtracting the known pure resistances of the 2.2 k Ω resistor and the NS in the bath.

We have assumed a series resistor-capacitor model for each metal-electrolyte interface, which is appropriate for applied voltages that are well below those required for electrolysis or corrosion (DE BOER and VAN OOSTEROM, 1978). The applied test voltages were about ± 0.1 VDC; residual polarisation voltages on the various electrode materials operated in this manner were all substantially less than ± 0.1 VDC with respect to a calomel reference electrode about 1 cm away in the bath, when measured occasionally within 3 s of testing. The measured interface properties seemed to be unaffected by naturally occurring and applied fluctuations within this range; the deliberate application of unphysiological steady polarisations and/or sinusoidal voltages larger than 0.4 V did have substantial effects on the measurements and was avoided.

3 Measurement of field potentials

3.1 Electrode bath

We constructed an idealised planar physical model for two arrangements of bipolar iridium electrodes (Fig. 2):

- (i) disk + disk: two flat circular electrodes, 0.250 mm in diameter and placed such that their nearest edges were 0.100 mm apart, simulating a closely spaced, radial bipolar arrangement;
- (ii) long + disk: one flat circular electrode (0.250 mm in diameter) placed 0.100 mm from the nearest edge of one long, thin electrode (0.250 mm wide, 12 mm long), simulating a novel design that would reduce the number of leads needed for a given number of radial bipolar stimulation sites.

The position of the disk electrodes was established by drilling holes (0.250 mm in diameter) in the Perspex base of the bath

* Voltech, UK; distributed by Rohde and Schwarz

using a precision numerically-controlled milling machine†. The position of the long electrode was established by milling a shallow groove (0.125 mm deep × 0.250 mm wide) in the surface of the bath. Fine iridium wires (0.250 mm diameter) were threaded through the holes until they were approximately flush with the surface of the bath, and a similar wire was placed into the groove. The wires were glued in place with acrylic adhesive. The surface of the bath was ground to bring the electrode contacts exactly flush with the Perspex surface and polished with 1200 grit abrasive to remove any surface irregularities. A circular ring (approximately 10 mm in diameter) was then glued to the surface to provide a bath that was filled with the PBS solution (Fig. 2b).

3.2 Impedance spectroscopy

We performed a series of impedance spectrograms on the disk + disk contacts at varying levels of iridium activation. The TF2000 frequency analyser was connected to a series arrangement of the bipolar contacts in PBS solution plus a small precision resistor (100 Ω) that provided the reference potential. Magnitude and phase angle of the impedance represented by the two contacts in PBS was measured for a logarithmic series of 20 frequencies from 60 Hz to 50 kHz applied at a constant voltage of 0.1 VRMS, similar to the voltages produced in the large-surface constant current bath. Owing to higher impedances encountered with the realistic electrodes, it was not practical to use the pseudo-constant current circuit described in Fig. 1a. Complete spectrograms were obtained for NAIR (defined as the freshly cathodically stripped surface after prior activation) and for activation periods of 1, 5, 15 and 50 min (the latter fully activated state was the AIR used for field measurements).

3.3 Field measurements

Sinusoidal signals at four different frequencies (300 Hz, 1 kHz, 3 kHz, 10 kHz) were applied to each of the stimulating

† Dynamite 2400

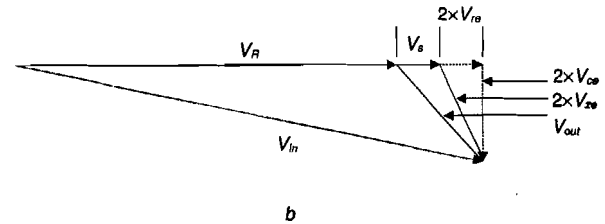
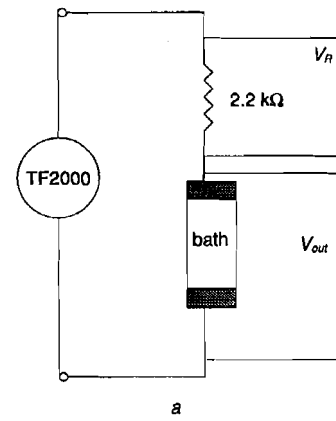


Fig. 1. (a) Schematic configuration for impedance spectroscopy of electrode materials in a cylindrical NS bath; (b) vector decomposition method used to obtain metal-electrolyte interface properties from test measurements; V_R = potential measured across series resistor; V_s = potential across saline in bath; V_{ze} = potential across both electrode interfaces; V_{re} = potential due to resistive components of electrode interface; V_{ce} = potential due to reactive component of electrode interface

electrode pairs by the TF2000. The stimulus voltage was set so as to maintain a charge density of 0.040 mC cm⁻² phase⁻¹ for each frequency. The resultant electrical fields in the PBS solution above the stimulating contacts were recorded by a Parylene-coated Ir microelectrode (LOEB *et al.*, 1977) with a

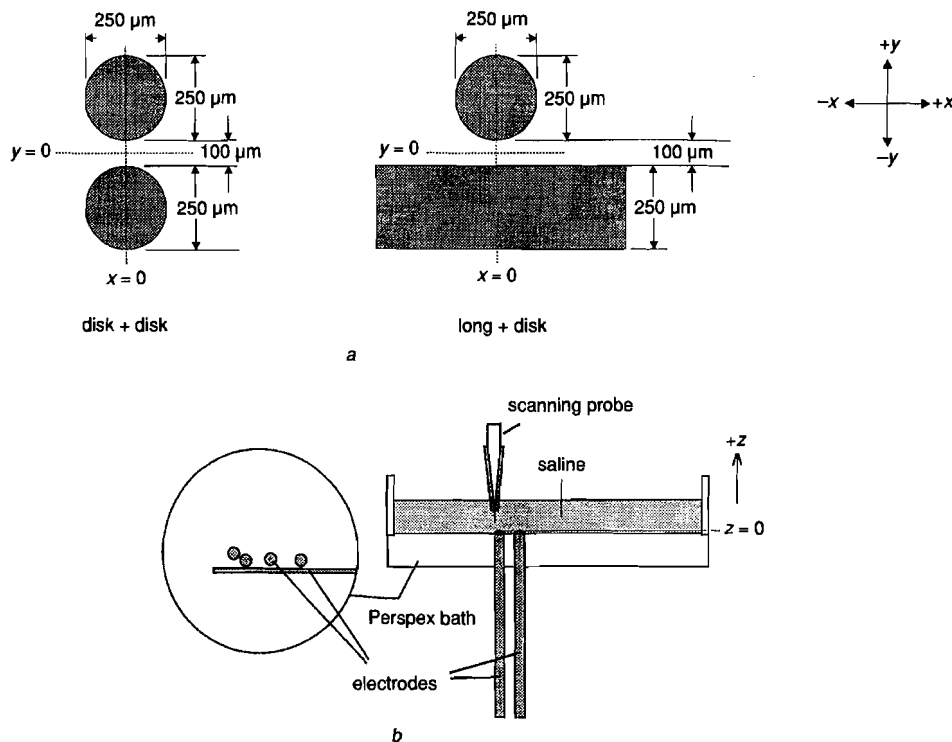


Fig. 2. (a) Top view electrode contact geometries and co-ordinate frames for idealised planar model of bipolar cochlear electrodes; (b) side view; physical construction of bath for scanning electrical fields above stimulating electrodes

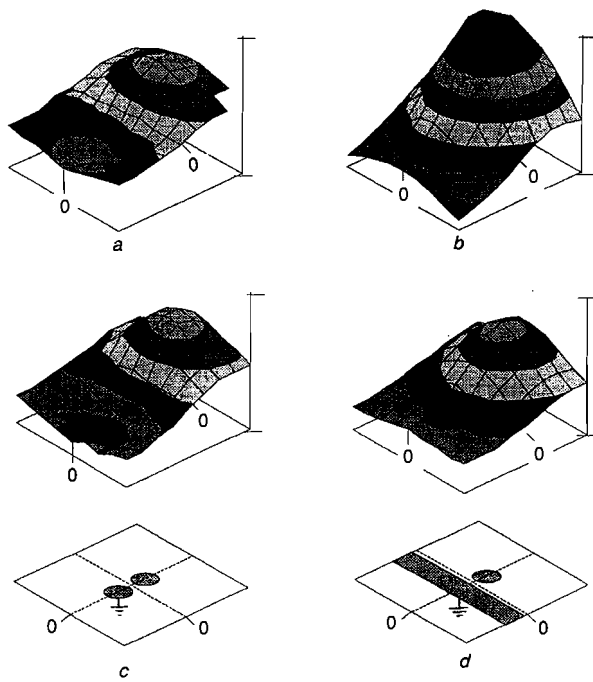


Fig. 3. Field potentials recorded in a planar grid 0.5 mm above the stimulating contacts with respect to the common contact (indicated by ground symbol), for 185 μA , 3 kHz sinusoid ($0.040 \text{ mC cm}^{-2} \text{ phase}^{-1}$); calibration bars = 8 mV; (a) NAIR disk + disk; (b) NAIR long + disk; (c) AIR disk + disk; (d) AIR long + disk

5 μm tip. The amplitude and phase of the field potentials were measured with respect to the common side of the stimulating pair (one of the two disk contacts or the long contact in the long + disk configuration).

The probe was moved through a series of measurement points on a series of rectangular grids (x, y axes defined in Fig. 2a) positioned parallel to and at various heights (z dimension: 0.025, 0.25, 0.5 and 1.0 mm) above the plane of the stimulating electrodes. The NC-milling machine was used as a programmable three-dimensional micromanipulator, controlled via its serial interface with a personal computer that also controlled the stimulation and measurement sequence of the TF2000. For brevity we present data from the $z = 0.50$ mm plane that reflects the typical distance between cochlear electrode contacts and the spiral ganglion cells in a human cochlea. The step size and extent of the grid was scaled to the z -axis value; for the data from the 0.5 mm plane that are presented in this paper, the step size was 0.2 mm over an extent of ± 0.8 mm for x and y .

3.4 Analysis

The absolute amplitudes of the waveforms sampled at the various points in each 2-D grid were plotted as 3-D contours with shaded isopotential regions (Fig. 3). These are useful for understanding the flow of current at various regions of the bath. In order to understand the efficacy and selectivity of these currents for stimulating neurons, we computed the potential gradients that would tend to affect the polarisation of the processes of the spiral ganglion cells, which are arranged parallel to the y -axis in our co-ordinate frame. The optimal orientation for radial bipolar electrodes would place one contact opposite the cell body of the spiral ganglion cell and the other opposite its distal dendrite, with an intercontact spacing about equal to the space constant of the neural process. Both stimulation electrode geometries tested here had intercontact spacings of 0.350 mm centre-to-centre, which is

probably on the same order as the space constant. (In fact, this intercontact spacing is severely limited by the available circumference of the cylindrical electrode array that can be inserted into the scala tympani, typically 0.6–1.0 mm in diameter.) To summarise the stimulus efficacy of a given electrode configuration and frequency, we chose the total potential gradient along the y -axis between the points directly over the centres of the two electrodes ($y = \pm 0.175$ mm). To determine the stimulus selectivity, we plotted the strength of this y -axis gradient at various distances away from the electrode centres along the x -axis (Figs. 4 and 5).

4 Results

4.1 Metal-electrolyte interface properties

The magnitude and phase of the impedance (Fig. 6a) and specific resistance and capacitance (Fig. 6b) attributable to a single metal/electrolyte interface were computed by vector decomposition for Pt, NAIR and IR foils in the cylindrical chamber. In general, all materials behaved like series RC circuits with frequency dependent values, resulting in decreasing magnitudes and phase angles at higher frequencies. AIR had the lowest, most resistive impedances and the least frequency dependence in its RC values. Pt had the highest impedance, dominated by its relatively low and highly frequency-dependent capacitance over the entire frequency range. NAIR was intermediate in impedance but the frequency dependence of the RC values was closer to Pt than AIR.

Impedance spectroscopy of the disk + disk electrode configuration revealed similar overall trends (Fig. 7) but important quantitative differences. The NAIR contacts had a much higher impedance than even the partially activated AIR (1 min) across the frequency spectrum. Both the magnitudes and phase angles of the NAIR impedance were somewhat variable across repeated measurements, and the phase angle versus frequency plot tended to plateau in the mid-range (1–10 kHz) rather than follow a simple asymptotic trend toward zero, as would be expected for a constant value capacitance. Such complex behaviour is typical of Warburg components. Activation for only 1 min produced only a tiny change in the cyclic voltammogram (compare 0 min cycle with 1 min cycle in Fig. 7b) but a large decrease in the magnitude and improvement in the stability of the impedance spectrograms. Further activation produced large changes in the cycle voltammograms but relatively small effects on the impedance spectroscopy that were confined mostly to the lower frequencies, as would be expected for increasing values of metal-electrolyte capacitance in series with a constant access resistance in the PBS. At the highest levels of activation (50 min), the asymptotic value of the impedance at the highest frequencies started to rise slightly, consistent with an increase in the access resistance through the growing thickness of iridium oxide on the electrode contacts. Note that, for intermediate activation times (5 and 15 min curves in Fig. 7), the shapes of the impedance magnitude and phase curves approach those associated with a simple series RC circuit with frequency-independent values, rather than a typical Warburg component.

4.2 Potential gradients over idealised electrodes

The amplitudes of the sinusoidal voltage obtained at a level 0.5 mm above the surface of the electrodes when stimulated at a frequency of 3 kHz were plotted for each combination of

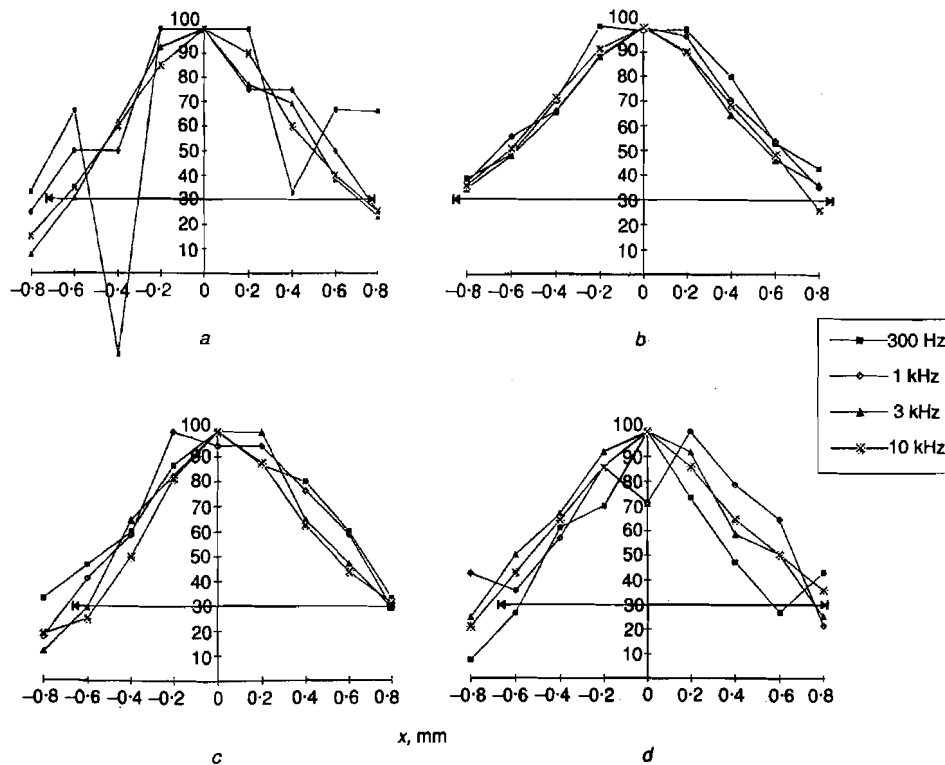


Fig. 4. Relative efficacy of stimulation longitudinally in the cochlea for four frequencies of sinusoidal stimulation applied to the same four electrode configurations as in Fig. 3; (a) NAIR disk + disk; $\lambda = 1.49$; (b) NAIR long + disk; $\lambda = 1.72$; (c) AIR disk + disk; $\lambda = 1.48$; (d) AIR long + disk; $\lambda = 1.50$; at -10 dB = 30%

the electrode material and geometry (Fig. 3a-d). The equipotential contours represent the electric field due to the current flow between the pairs of electrodes. Perhaps the most notable finding is that the different electrode geometries had a great effect on the fields produced by the NAIR but very little effect with AIR. In the case of the very low impedance AIR electrode, the distribution of current density through the metal-electrolyte interface tended to be dominated by series resistance of the PBS solution between the contacts. Thus, most of the current flowed between the closely approximated edges and stayed close to the plane of the contacts, which was

a relatively long distance from the plane of measurement provided in Fig. 3. At this distance ($z = 0.5$ mm), the potential field plots are similar in amplitude and shape over the driven AIR disk electrode in both geometries; the main difference is the slight concavity seen over the common disk electrode in the disk + disk geometry but missing over the elongated common electrode in the long + disk geometry. For the NAIR contacts, the change from disk + disk to long + disk is accompanied by a marked increase in the amplitude of the potentials and a marked convexity over the elongated common electrode. This results from the fact that the current

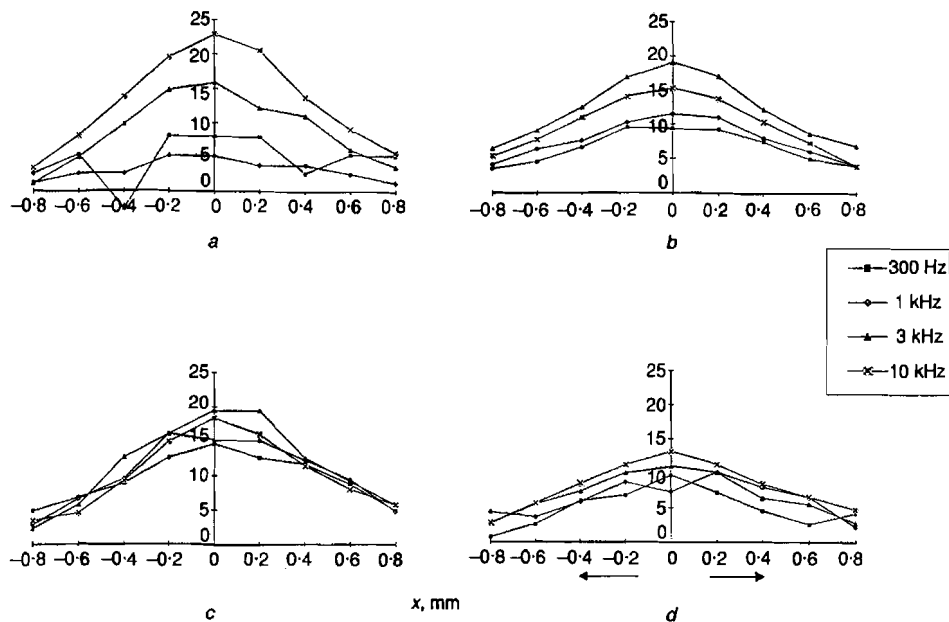


Fig. 5. Same data as Fig. 4, normalised to stimulus current to show effects of different electrode configurations on relative efficacy of stimulation along the x-axis; (a) NAIR disk + disk; (b) NAIR long + disk; (c) AIR disk + disk; (d) AIR long + disk

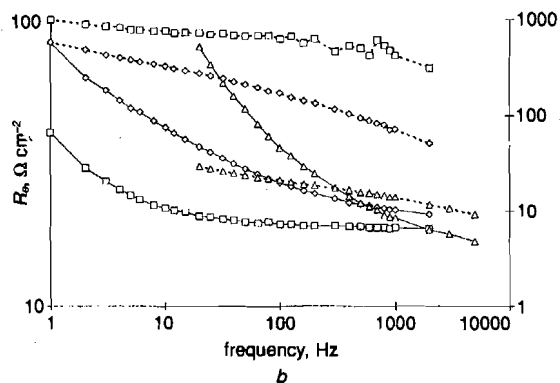
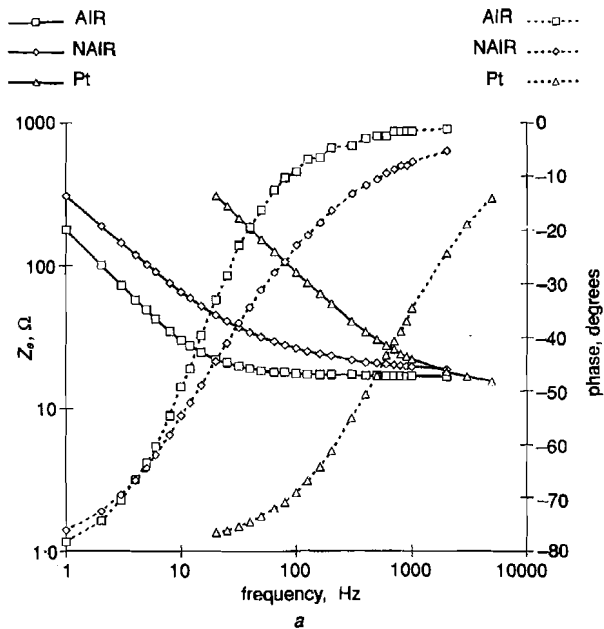


Fig. 6. (a) Impedance spectroscopy of three candidate electrode materials (Pt=pure platinum; AIR=activated iridium; NAIR=non-activated iridium), showing amplitude (solid lines, reference to left abscissa) and phase (dashed lines, reference to right abscissa). (b) specific resistivity (solid lines, left abscissa) and capacitance (dashed lines, right abscissa) for the same three materials

density is more evenly distributed over both electrodes and is thus less confined to the PBS layers close to the plane of the contacts. Such a distribution would be more efficient in terms of depolarising neurons lying near the $z=0.5$ mm plane, but would it be more selective?

The y -gradient plots in Fig. 4 indicate that the AIR and NAIR materials should result in similarly localised recruitment for both disk + disk configurations. The plots are normalised to the maximal gradient to simulate the effects of the fitting process, whereby each electrode site in a patient is scaled according to the stimulus strength required to reach perceptual threshold for each frequency of stimulus. The horizontal bar added to each plot indicates λ , the physical distance along the x axis at which the strength of the y -gradient has decayed to 30% of the peak value (10 dB attenuation; taken as the mean for all frequencies to minimise the effects of noise). For the long + disk configurations, the NAIR gradients are less well localised along the x axis (parallel to the long contact and to the axis of the basilar membrane *in situ*). The effect is slightly greater for the lower frequencies (note 300 Hz curve in Fig. 4b), where the limited capacitance of the NAIR leads to a high metal-electrolyte interface impedance that prevents the development of high current densities between the

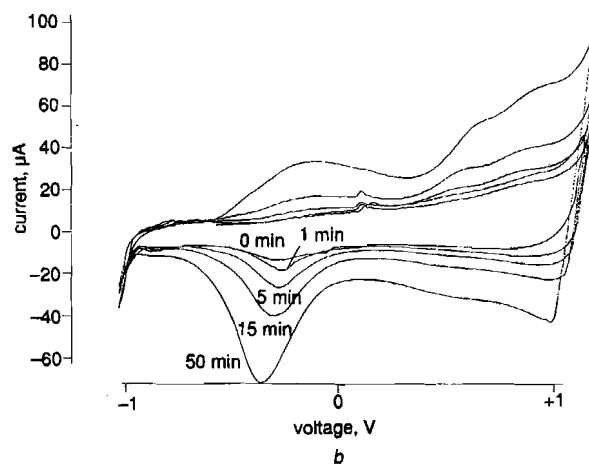
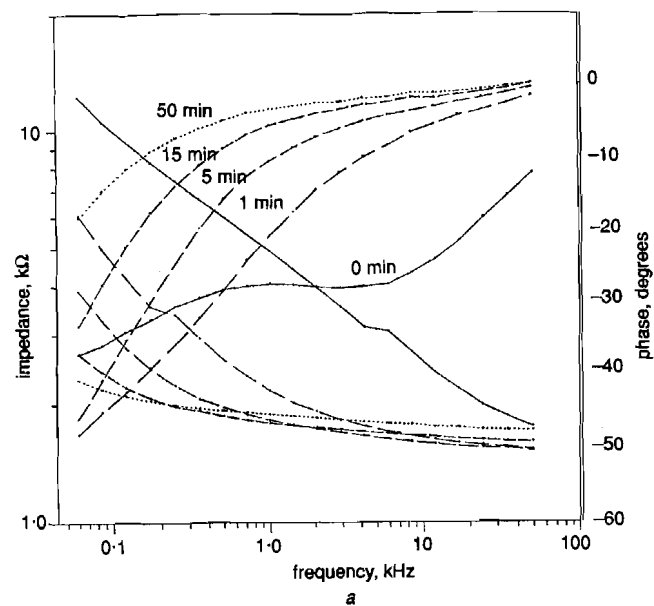


Fig. 7. (a) Impedance spectroscopy of iridium disk + disk contacts in the non-activated state (0 min) and after various durations of cyclic activation (1, 5, 15 and 50 min labels on phase curves and corresponding line types of impedance magnitude curves); (b) cyclic voltammograms for corresponding states of iridium disk + disk contacts

two apposed edges. Note that the low frequency curves tend to be quite noisy because they actually reflect much lower absolute currents required to maintain constant charge density across all frequencies, resulting in much lower field potentials in the bath.

The plots in Fig. 4 have been normalised for the maximal y gradient for each frequency to identify frequency dependent effects on the shapes of the gradients. The plots in Fig. 5 have been normalised according to applied stimulus current, which is usually the controlled parameter in cochlear stimulation. Thus, Fig. 5 can be used to anticipate the waveform distortion that would result from applying a complex waveform containing a range of frequency components. The actual amplitude of the y gradient sampled over the 0.350 mm interelectrode distance depends complexly on the interfacial impedance for that frequency and the z axis distance above the plane at which the y gradient is computed. The general finding (illustrated in Fig. 5 for $z=0.5$ mm) is that NAIR exhibits complex frequency and electrode geometry dependencies because its interfacial impedance is not negligible at these dimensions. AIR is such a low impedance interface across all frequencies that the potential gradients are dominated by the purely resistive impedance of the PBS bath.

4.3 Effects of phase gradients

The reactive nature of the impedance of the metal-electrolyte interface gives rise to small phase differences between the electric fields recorded at various locations over the electrodes. The effective stimulus gradient is not the difference between the peak-to-peak amplitudes of two such stimulus waveforms (as computed above for simplicity) but rather is related to the instantaneous differences in potential between the waveforms at the two sites. As we are using sinusoidal stimulation, the instantaneous gradients between two adjacent points whose waveforms are out of phase will vary throughout one cycle of the signal. The effect on membrane polarisation of a neuron spanning such a time-varying gradient is effectively integrated over each half-cycle of the sinusoidal waveform. This can be thought of graphically as the area between the actual waveforms (including phase differences) of the sinusoidal stimulus potentials recorded at any two sites. The effect of extracellular potential gradients on membrane polarisation is actually related to the first derivative (dV/dt) of those potential gradients (RANCK, 1975), but the derivative of a sine wave is also sinusoidal, and so the simple integral still applies.

The phase differences between the recorded waveforms and the reference applied waveform are shown in Fig. 8a for various locations on the $z=0.5$ mm plane over the long + disk configuration of AIR contacts at 3 kHz. The phase differences are maximal directly over the active contact (disk) as would be expected, but they never exceed 8° . In order to assess their effects, we have plotted the half-cycle integrals of the local voltage gradient along the y axis at each of the data points (not to be confused with the y gradient described earlier, which spans the entire distance between the centre-axes of the two contacts). In Fig. 8b, these were computed on the basis of amplitude alone, ignoring the phase differences, according to the equation:

$$\int_0^{T/2} (A_y \sin t - A_{y+\Delta y} \sin t).dt$$

where A_y is the amplitude of the field at point y and $A_{y+\Delta y}$ is the amplitude of the field at the adjacent point

In Fig. 8c, these were computed from the waveforms according to both amplitude and phase, according to the equation

$$\int_{t_1}^{t_2} A_y \sin(t + \theta_y) - A_{y+\Delta y} \sin(t + \theta_{y+\Delta y}).dt$$

where A_y is the amplitude of the field at point y , θ_y is the phase of the field at point y (relative to the input signal) $A_{y+\Delta y}$ is the amplitude of the field at the adjacent point, $\theta_{y+\Delta y}$ is the phase of the field at the adjacent point (relative to the input signal) t_1 is the first crossing point of the two signals and t_2 is the second crossing point of the two signals.

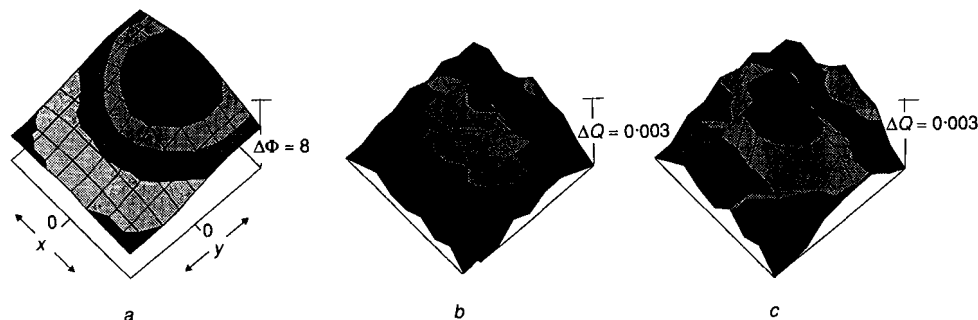


Fig. 8. (a) Plot of phase angle of electrical fields recorded in grid at $z=0.5$ mm above plane of long + disk AIR contacts with respect to 3 kHz stimulus waveform; (b) map of local gradients of electrical field strength in the y axis assuming uniform phase; (c) similar map of local gradients including phase differences from (a)

In both Figs. 8b and 8c, the steepest voltage gradients in the y axis tend to occur near the origin, which is centred between the two contacts. However, failure to consider phase differences tends to underestimate the amplitude and extent of this voltage gradient by about 50% for the particular conditions of these measurements, even though the phase angles are all largely resistive. Note that the total y gradients presented in Figs. 4 and 5 are equivalent to spatial integrals of the local gradients presented in Fig. 8, where the integral covers the span $y = \pm 0.175$ mm. Distributions of phase gradients, such as those shown in Fig. 8a, would be expected to be larger for conditions in which the capacitive reactance contributing to the total impedance is larger, e.g. for lower frequencies and for NAIR or Pt stimulating electrodes.

5 Discussion

5.1 Implications for multichannel designs

The long + disk configuration permits an electrode design in which the number of separately wired contacts required to achieve N radial bipolar sources is only $N + 1$, rather than the $2N$ required for the disk + disk configuration. This could be used to reduce the complexity of electrode fabrication and multichannel hermetic feedthroughs on cochlear prostheses, or it could be used to increase the number of parallel independent channels. The region along the cochlea in which the speech frequencies are mapped is about 14 mm in length (spanning characteristic frequencies of about 5 kHz at 10 mm in depth to about 300 Hz at 24 mm in depth). This would accommodate 15 sites at 1 mm intervals. The analysis in Fig. 3 suggests that these sites would overlap somewhat in their recruitment of neurons, particularly at the high end of the typical dynamic range of 12–20 dB for each site, but that this problem could be minimised by the use of AIR contacts (reducing λ). Moving the plane of analysis closer to the plane of the electrodes (z axis) also tends to increase the peak amplitude and reduce λ , suggesting that effective designs must consider both the arrangement of contacts on the electrode surface and the position which the electrode array comes to assume in the scala tympani.

It is also possible that the overlap could be used to advantage to create virtual electrodes by deliberately stimulating two adjacent disk electrodes simultaneously so that their y gradients would sum to a peak somewhere between the two longitudinal sites. λ depends on the exact geometry of the electrode contacts, the degree of activation of the iridium and the frequency spectrum of the stimulus waveform. In the examples analysed here, the iridium was heavily activated and the contacts were relatively large and close together at their edges. For a lesser degree of activation and for different geometries, the frequency at which λ starts to increase for

long + disk electrodes could be shifted to the higher frequencies comprising most of the energy in the brief biphasic pulses used in the continuous interleaved sampling strategy (WILSON *et al.*, 1991). Systematic changes in pulse width could be used to fine-tune λ to compensate for differences in the condition of the spiral ganglion cells or placements of the electrode within the scala tympani of a given patient.

An exhaustive examination of the many interactive factors that influence electrode design would be impractical using physical model systems such as that employed in this study. Furthermore, such model systems cannot capture the subtleties of the heterogeneous and anisotropic conductances of the normal tissues surrounding the typical cochlear electrode *in situ*. The next stage of this process is to use the characterisation data for the metal-electrolyte interface to develop realistic finite element models that incorporate both the tissue and the interface properties in order to evaluate candidate designs for new cochlear electrodes and stimulus waveforms. A quantitative comparison of the spectroscopy data in Figs. 6 and 7 reveals an important complication for this process. If we assume that the asymptotic value of disk + disk impedance at the higher frequencies (50 min curve in Fig. 7a) reflects the series resistance of the fluid between them, this frequency-independent term can be subtracted from the complex impedance at the lower frequencies to estimate the magnitude of the capacitance presented by the two metal-electrolyte surfaces in series. The resulting reactance at 60 Hz is 0.7 or 0.35 k Ω per contact. Each contact has a geometric surface area of 0.05 mm². Assuming a simple capacitor distributed equally across the contact surface, this corresponds to 7.6 μ F, or a specific capacitance of 15,100 μ F cm⁻². This is about 15 times the specific capacitance of about 1000 μ F cm⁻² computed for the specularly polished AIR foil used in the cylindrical characterisation bath (Fig. 6b). Presumably, this difference is caused by the relatively coarse surface polishing of these contacts, which produced a visibly scratched surface under the microscope.

The actual surface finish of contacts in real cochlear electrodes will depend on many factors involved in their original preparation, handling during fabrication and final exposure, cleaning and testing procedures. In order to use electrode models effectively, it will be necessary to scale the specific interfacial properties for a range of possible surface finishes and to develop processes to control these finishes in production within a range for which the model predicts the desired field distributions. In our experience with these electrode geometries, the characteristics of AIR were more predictable and stable than NAIR and especially Pt, which depended on factors such as the accumulation or stripping of oxides by previous testing or cathodic bubbling (note the unusual shape of the phase plot for NAIR in Fig. 7a, which reverted to a more typical shape after 1 min activation). However, the long-term stability of AIR electrodes in body tissues remains to be demonstrated. In practice, the relatively large and frequency-independent capacitance observed for AIR under these conditions of use may simplify matters by making the interface impedance negligible compared to the resistance, which depends only on the geometry and resistivity of the surrounding tissues. The measurements reported here, however, should not be extrapolated to other electrode geometries and stimulus frequencies and amplitudes without empirical validation. AIR can demonstrate much more complex properties, particularly for operating voltages, frequencies and oxide thicknesses for which access resistance through the oxide itself becomes relatively large (GLARUM and MITCHELL, 1993).

5.2 Implications for power consumption and safety

The materials and geometries that tend to produce the most localised potential gradients for stimulation (closely spaced bipolar AIR contacts) also require the largest applied currents. This is a necessary consequence of using a bipolar geometry to stimulate selectively neurons that lie some distance from the plane of the contacts; selectivity depends on sharply falling fringe effects of high-current shunts between the closely spaced contacts. As the other components of cochlear prosthetic systems become more power efficient (digital speech processors, pulse generating circuits, RF transmission links etc.), the power dissipated in the electrodes themselves becomes the limiting factor in the trade-off between battery size and life. The compliance voltage that must be provided to drive the necessary current through the electrode contacts is also an important limitation in the selection of integrated circuit processes. This voltage must be set high enough to deal with the highest impedance that can occur, a problem compounded by the tendency of conventional Pt-Ir alloy electrodes to drift into high impedance states if unstimulated for some period of time (DORMAN *et al.*, 1992). AIR offers a substantial reduction in the impedance of the metal-electrolyte junction over the platinum-based contacts now in use (see Fig. 6), an effect that is already being used in other low-power bio-stimulation applications (LEE *et al.*, 1991; DELBUFALO *et al.*, 1993; ADLER *et al.*, 1990). AIR impedances were also less labile during our *in vitro* tests, although it remains to be seen if this advantage persists *in vivo*.

It is also important to consider the possibility of reaching safety limits for safe charge injections in the localised edge regions where the contacts experience high-current densities (SUESSERMAN *et al.*, 1991). The fundamental properties of AIR, as compared to platinum, are again encouraging. The AIR charge density limit is at least a factor of ten higher than that of the platinum-iridium contacts now in widespread use in cochlear prostheses. Furthermore, the edge-effect electrode has a tendency to self-adjust; as working voltages are increased to achieve higher charge transfers per phase, the current distribution automatically spreads out over the remainder of the relatively large contact area that is available.

Acknowledgments—This research was supported by NIH Program Project Grant 5P01-DC00036.

The authors would like to thank the other members of the program team, in particular the director of the team Dr. Charles Finley, Research Triangle Institute, for their advice and guidance; and Ray Peck, Roy Young and Derek Cooke, Jr, Queen's University, for their technical assistance.

References

- ADLER, S., SPEHR, P., ALLEN, J. and BLOCK, W. (1990): 'Chronic animal testing of new cardiac pacing electrodes,' *Pace. Pac. Clin. Electrophys.*, **13**, pp. 1896-1900
- DE BOER, E. and VAN OOSTEROM, A. (1978): 'Electrical properties of platinum electrodes: Impedance measurements and time-domain analysis,' *Med. Biol. Eng. Comput.*, **16**, pp. 1-10
- DELBUFALO, A. G. A., SCHLAEPFER, J., FROMER, M. and KAPPENBERGER, L. (1993): 'Acute and long-term ventricular stimulation thresholds with a new, iridium oxide-coated electrode,' *Pace. Pac. Clin. Electrophys.*, **16**, pp. 1240-1244
- DORMAN, M. F., SMITH, L. M., DANKOWSKI, K., MCCANDLESS, G. and PARKIN, J. L. (1992): 'Long-term measures of electrode impedance and auditory-thresholds for the Ineraid cochlear implant,' *J. Speech Hear. Res.*, **35**, pp. 1126-1130
- EDDINGTON, D. K. (1980): 'Speech discrimination in deaf subjects with cochlear implants,' *J. Acoust. Soc. Am.*, **68**, pp. 885-891

- FINLEY, C., WILSON, B. and WHITE, M. (1990): 'Models of neural responsiveness to electrical stimulation' MILLER, J., and SPELLMAN, F. (Eds.): *in Cochlear implants-models of the electrically stimulated ear* (Springer Verlag, New York). pp. 55-96
- FINLEY, C., (1989): 'A finite element model of radial bipolar field patterns in the electrically stimulated cochlea; two and three dimensional approximations and tissue parameter sensitivities.' IEEE 11th Ann. Conf. of the Engineering in Medicine and Biology Society
- GEDDES, L. A. (1972): 'Electrodes and measurement of bioelectric events' (Wiley Interscience, New York)
- GEDDES, L. A., DA COSTA, C. P. and WISE, G. (1970): 'The impedance of stainless steel electrodes,' *Med. Biol. Eng.*, **9**, pp. 511-521
- GLARUM, S. H., and MARSHALL, J. H. (1980): 'The A-C response of iridium oxide films,' *J. Electrochem. Soc.*, **127**, pp. 1467-1474
- LEE, I. S., BUCHANAN, R. A. and WILLIAMS, J. M. (1991): 'Charge-injection densities of iridium and iridium-ion-implanted Ti-6Al-4V with relevancy to neural stimulation,' *J Biomed. Mater. Res.*, **25**, pp. 1039-1043
- LOEB, G. E., BAK, M. J., SALCMAN, M., and SCHMIDT, E. M. (1977): 'Parylene as a chronically stable, reproducible microelectrode insulator,' *IEEE Trans.*, **BME-24**, pp. 121-128
- LOEB, G. E., BYERS, C. L., REBSCHER, S. J., CASEY, D. E., FONG, M. M., SCHINDLER, R. A., GRAY, R. F. and MERZENICH, M. M. (1983): 'The design and fabrication of an experimental cochlear prosthesis,' *Med. Biol. Eng. Comput.*, **21**, pp. 241-254
- MAYER, S., GEDDES, L. A., BOURLAND, J. D. and OGBORN, L. (1992): 'Faradic resistance of the electrode electrolyte interface,' *Med. Biol. Eng. Comput.*, **30**, pp. 538-542
- MERZENICH, M. M., WHITE, M., VIVION, M. C., LEAKE-JONES, P. A. and WALSH, S. M. (1979): 'Some considerations of multi-channel electrical stimulation of the auditory nerve in the profoundly deaf; interfacing electrode arrays with the auditory nerve array,' *Acta Oto. Laryngol.*, **87**, pp. 196-203
- ONARAL, H. P. and SCHWAN, M. A. (1982): 'Linear and non-linear properties of platinum electrodes polarization. Part 1: Frequency dependence at very low frequencies,' *Med. Biol. Eng. Comput.*, **20**, pp. 299-306
- RANCK, J. B., Jr. (1975): 'Which elements are excited in electrical stimulation of mammalian central nervous system: A review,' *Brain Res.*, **98**, 417-440
- ROBBLEE, L. S., LEFKO, J. L. and BRUMMER, S. B. (1983): 'Activated Ir: An electrode suitable for reversible charge injection in saline solution,' *J Electrochem. Soc.*, **130**, pp. 731-733
- SUOSSERMAN, M. F., SPELMAN, F. A. and RUBINSTEIN, J. T. (1991): 'In vitro measurement and characterization of current density profiles produced by nonrecessed, simple recessed, and radially varying recessed stimulating electrodes,' *IEEE Trans.*, **BME-38**, pp. 401-408
- WILSON, B., FINLEY, C., LAWSON, D., WOLFORD, R., EDDINGTON, D. and RABINOWITZ, W. (1991): 'Better speech recognition with cochlear implants,' *Nature*, **352**, pp. 236-238